Applied Catalysis B: Environmental 187 (2016) 375–385

Contents lists available at ScienceDirect

Applied Catalysis B: Environmental

journal homepage: www.elsevier.com/locate/apcatb

Production of high-grade diesel from palmitic acid over activated carbon-supported nickel phosphide catalysts

Hui Xin [a], Kai Guo [b], Dan Li [b,**], Huaqing Yang [a,*], Changwei Hu [b]

[a] College of Chemical Engineering, Sichuan University, Chengdu, Sichuan 610065, PR China
[b] Key Laboratory of Green Chemistry and Technology, Ministry of Education, College of Chemistry, Sichuan University, Chengdu, Sichuan 610064, PR China

ARTICLE INFO

Article history:
Received 9 September 2015
Received in revised form 20 January 2016
Accepted 22 January 2016
Available online 25 January 2016

Keywords:
Deoxygenation
Palmitic acid
Nickel phosphide

ABSTRACT

A series of activated carbon (AC)-supported nickel phosphide catalysts were prepared; characterized using XRD, XPS, TEM, and NH_3-TPD techniques; and evaluated for the deoxygenation of palmitic acid. The formation of Ni_2P and/or $Ni_{12}P_5$ on the surface of AC could be controlled by controlling the Ni/P molar ratios. With low Ni/P molar ratios from 0.5 to 0.8, only crystalline Ni_2P formed. Both Ni_2P and $Ni_{12}P_5$ formed with Ni/P ratios of 1.0 and 1.5, whereas only $Ni_{12}P_5$ formed with a Ni/P ratio of 2.0. As the Ni/P ratio further increased (Ni/P $\geq$ 3.0), crystalline Ni formed in addition to $Ni_{12}P_5$. The deoxygenation activities of the Ni_xP/AC catalysts were strongly dependent on the types and dispersion of the nickel phosphide. The oil yield and C_{15} selectivity on the catalysts followed the sequence $Ni_{1.5}P/AC > Ni_{2.0}P/AC > Ni_{1.0}P/AC \approx Ni_{3.0}P/AC > Ni_{4.0}P/AC > Ni_{0.5}P/AC \approx Ni_{0.8}P/AC$, $Ni_{1.0}P/AC > Ni_{1.5}P/AC \approx Ni_{0.8}P/AC > Ni_{0.5}P/AC \approx Ni_{2.0}P/AC > Ni_{3.0}P/AC > Ni_{4.0}P/AC$, respectively. The high activity was attributed to the coexistence and high dispersion of Ni_2P and $Ni_{12}P_5$, which were favorable for branched alkanes formation, C_{15} selectivity improvement and oil yield increase. Due to the high-grade diesels (HV = 46.5 MJ kg^{-1}) obtained, Ni_xP/AC can be considered to be a very promising catalyst for transforming fatty acids into high-grade diesel.

1. Introduction

Declining fossil fuels and increasing environmental problems, including global warming and air pollution, are driving our society to search for new sustainable sources of liquid fuels. Fatty acids are produced from the hydrolysis of triglycerides in animal fats and plant oils, which constitute an important renewable biofuel feedstock. Accordingly, biofuel has been proposed as a desirable substitute because it is renewable, carbon-neutral and inexpensive. However, to obtain high-grade fuel, the low stability, high viscosity, and poor calorific value of the feedstock should be improved. These drawbacks are caused by the high oxygen content in their molecular structures [1–4]. Therefore, removing oxygen from the feedstock is becoming one of the most significant issues to obtain high-grade fuel that can potentially serve as or be converted to a drop-in replacement for the fuel currently in use. Currently, three approaches have been used to remove oxygen from fatty acids as shown in Scheme 1 [5–7], in which the degree of H_2 consumption follows the order of decarboxylation < decarbonylation < hydrodeoxygenation (Scheme 1).

There have recently been many reports on the heterogeneous catalytic deoxygenation of fatty acids, and good overviews are available [8–10]. Typically, the most active heterogeneous catalysts are noble metals (Pt, Pd) on a high-surface-area support (carbon-based support) [11,12]. In fact, carbon materials as supports have triggered increasing interest in applications of catalytic deoxygenation due to their uniform mesoporous structures, high surface areas and inert surfaces [11–14]. Fu et al. showed that Pt/C and Pd/C catalysts are highly active for the hydrothermal decarboxylation of different saturated and unsaturated fatty acids [13,14]. Although supported Pd and Pt catalysts have been found to be effective in the conversion of fatty acids and their derivatives into diesel-like hydrocarbons, their high cost has motivated the continuous development of low-cost substitutes. According to the activity trends of Pd > Pt > Ni > Rh > Ir > Ru > Os, Snåre et al. suggested that Ni-based catalysts could be promising candidates [15]. Nickel has been extensively studied for the deoxygenation of fatty acids, but it is not an attractive metal because it favors the cracking reaction [16–18]. Chen et al. demonstrated that Ni_2P/SiO_2 provided higher total selectivity to *n*-C_{11} and *n*-C_{12} in the deoxygenation of methyl

* Corresponding author at: Sichuan University, No. 24 South Section 1, Yihuan Road, Chengdu 610065, PR China.
** Corresponding author.
E-mail addresses: danli@scu.edu.cn (D. Li), huaqingyang@scu.edu.cn (H. Yang).

http://dx.doi.org/10.1016/j.apcatb.2016.01.051
0926-3373/

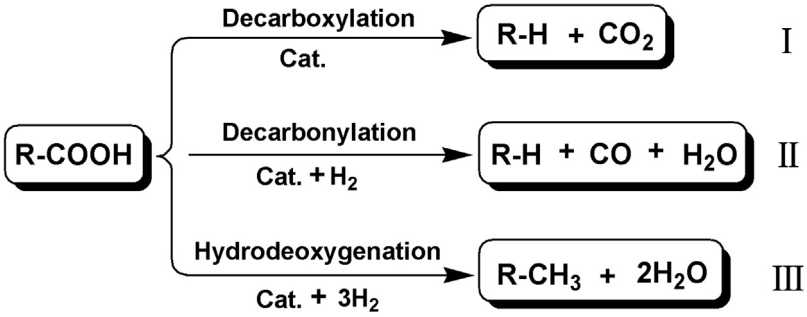

Scheme 1. The three pathways proposed for the deoxygenation of a fatty acid into hydrocarbons. The degree of consumption of H_2 follows the order of decarboxylation (I) < decarbonylation (II) < hydrodeoxygenation (III).

laurate than Ni/SiO_2, whereas Ni produced more cracked products [18a]. Yang et al. comparatively investigated the catalytic performances of Ni_2P/SBA-15 and Ni/SBA-15 toward the deoxygenation of methyl oleate, and they found that Ni_2P/SBA-15 exhibited higher catalytic decarboxylation activity than Ni/SBA-15. Thus, Ni_2P/SBA-15 was suggested to be a promising catalyst for the production of green diesel [17]. In this way, it was determined that transition metal phosphides exhibited particular deoxygenation activity.

To date, some researchers have used Ni_2P as a deoxygenation catalyst [17–22] and found that Ni_2P-based catalysts exhibited excellent catalytic deoxygenation performance. Yang et al. reported that Ni_2P particles can be distributed rather uniformly inside the SBA-15 channels, and the resulting catalyst exhibited an enhanced selectivity for hydrodeoxygenation products compared with Ni/SBA-15 [17]. Moreover, dispersing metal phosphides on mesostructured supports could further enhance their hydrotreating performance, as reported for the HDS of dibenzothiophene and the HDN of methyl aniline over Ni_2P supported on SBA-15 and KIT-6 [23]. In a recent work, we found that unsupported $Ni_{12}P_5$-containing catalysts are more active for the decarboxylation and decarbonylation of palmitic acid, compared with unsupported Ni_2P-containing catalysts [8a].

In the present work, we investigated in detail the effect of the nickel-to-phosphorus molar ratio on the formation and dispersion of different nickel phosphide species and on the deoxygenation performance using palmitic acid as a model compound.

2. Experimental

2.1. Catalyst preparation

The catalysts were prepared by incipient wetness impregnation. For all catalysts, the content of Ni was fixed at 24.2%. To control the formation of different nickel phosphide species (Ni_2P, $Ni_{12}P_5$, and $Ni_2P/Ni_{12}P_5$ mixture), the molar ratios of Ni/P were changed by adjusting the content of P. The controlled Ni/P molar ratios were 0.5/1, 0.8/1, 1.0/1, 1.5/1, 2.0/1, 3.0/1 and 4.0/1. The AC supports were purchased from the Jiangsun Nantong Activated Carbon Cooperation (China). Prior to impregnation, the AC samples were immersed in 1 M/L $NH_3{\cdot}H_2O$ for 18 h and then washed with distilled water until a neutral pH was achieved. Then, the resulting samples were dried at 373 K for 12 h and calcined at 873 K for 4 h under a nitrogen atmosphere. The dried samples were sieved to 40–60 mesh. The carbon supports (6 g) were impregnated with an aqueous solution containing 9.40 g of $Ni(NO_3)_2{\cdot}6H_2O$ and different amounts of $NH_4H_2PO_4$ for 24 h. Then, the samples were dried at 373 K for 12 h and calcined at 873 K under a nitrogen atmosphere for 4 h. The precursor sample was reduced under flowing H_2 (30 mL/min) to obtain the active phosphide catalyst. The reduction temperature was increased from room temperature to 873 K at a rate of 2 K min^{-1} and was maintained at this temperature for 2 h. Subsequently, the gas was switched to nitrogen, followed by cooling to room temperature. Finally, the carbon-supported catalysts were passivated in an air flow overnight at room temperature. The obtained samples were denoted as Ni_xP/AC catalysts (x = 0.5, 0.8, 1.0, 1.5, 2.0, 3.0, 4.0). The content of Ni was calculated using Eq. (1):

$$\text{Wt.\%Ni} = [\text{weightofNi}/(\text{weightofNi} + \text{weightofAC})] \times 100\%. \quad (1)$$

2.2. Catalyst characterization

X-Ray diffraction (XRD) patterns were recorded using a DX-1000 X-ray diffractometer equipped with Cu-Kα radiation. The X-ray tube was operated at 40 kV and 25 mA. Powder diffraction patterns were recorded over a 2θ range of 30–80 at a scan rate of 0.06 s^{-1}.

N_2 physisorption isotherms of the samples were measured at 77 K on a Micromeritics Tristar II 3020 analyzer. The surface areas were determined by the Brunauer–Emmett–Teller (BET) equation. The pore volumes and average pore diameters were determined by the Barrett–Joyner–Halenda (BJH) method from the desorption branches of the isotherms.

X-Ray photoelectron spectroscopy (XPS) experiments were performed on an AXIS Ultra DLD (KRATOS) spectrometer using a pass energy of 50 eV (0.1 eV per step). A monochromatic Al-Kα X-ray source was used as the excitation source, and the binding energy (BE) was calibrated using C1s at 284.6 eV. A Shirley background was subtracted from all spectra and peak fitting was performed using an 80/20 Lorentz-Gauss function.

Transmission electron microscopy (TEM) images of the samples were obtained on an FEI Tecnai G2 20 TWIN instrument at an acceleration voltage of 200 kV. An energy-dispersive X-ray (EDX) instrument was attached to the TEM system.

The acidities of the catalysts were evaluated by NH_3-temperature-programmed desorption using 1 vol.% NH_3 with He as the carrier gas, a heating rate of 10 K min^{-1} and over the temperature range of 373–773 K. The desorbed NH_3 was detected using a multifunction chemisorption analyzer and detected by a thermal conductivity detector (TCD). The detailed procedure of NH_3-TPD can be found in reference [8a].

Carbon monoxide (CO) chemisorptions and CO-TPD measurements were also performed using the Micromeritics Autochem II 2920 instrument. Approximately 0.1000 g of catalyst was degassed in 60 mL/min He at room temperature for 30 min. Prior to the measurements, samples were heated from room temperature to 650 K in a 60 mL/min flow of H_2 for 2 h. Prior to the chemisorption measurement, all of the samples were then degassed at 650 K in 45 mL/min He for 1 h. CO chemisorption were measured by injecting a calibrated sample volume of CO gas at 1 min intervals into a He flow (45 sccm/min) passing over the catalyst sample until CO uptake ceased. Catalyst samples were maintained at 273 K during

CO chemisorption measurements [8b]. When CO chemisorptions were obtained, and then CO-TPD experiments were carried out.

2.3. Catalytic deoxygenation of palmitic acid

The deoxygenation of palmitic acid was conducted in a fixed-bed reactor at 623 K for 2.5 h [8a]. For each run, the catalyst (3.0 g) was mixed with SiO_2 to improve heat transfer and to ensure a sufficient catalyst-bed length of 4 cm. The carrier gas was 5% H_2/Ar with a flow rate of 30 mL/min. Moreover, the deoxygenation reaction was carried out in atmospheric pressure and the volumetric rate of palmitic acid was 120.0 $cm^3\ h^{-1}$ according to the equation: $pV = nRT$.

The conversion (X) of palmitic acid was calculated using Eq. (2):

$$X = (W_1 - W_2)/W_1 \times 100\% \quad (2)$$

where W_1 and W_2 are the weights of added and unconverted palmitic acid, respectively. When the products were solid, the amount of unconverted palmitic acid in the products was also included in W_2.

The oil yield (Yield) was calculated by Eq. (3):

$$\text{Yield} = (W_{\text{Products}} - W_{\text{water}})/(W_1 - W_2) \times 100\%. \quad (3)$$

where W_{Products} and W_{water} are the weights of the total products and water generated in the reaction, respectively.

2.4. Product analysis

The liquid products were identified using gas chromatography-mass spectrometry (GC–MS, Agilent 5973) equipped with a capillary column (HP-INNOWAX, 30 m × 0.25 mm × 0.25 μm). The injector and detector temperatures were both set at 553 K. The temperature program for the GC oven was set as follows: 343 K (4 min), 5 K min^{-1}, 373 K (6 min), 10 K min^{-1}, 433 K, 10 K min^{-1}, 503 K (6 min).

The liquid products were quantitatively analyzed using a gas chromatograph (GC, FULI 9750) equipped with a capillary column (DB-5, 30 m × 0.25 mm × 0.25 μm) and a flame ionization detector (FID). N_2 was used as the carrier gas. The injector and detector temperatures were both set at 553 K. The temperature program for the GC oven used for analysis was as follows: 343 K (3 min), 5 K min^{-1}, 433 K (3 min), 10 K min^{-1}, 503 K (6 min).

The compositions of the gaseous products were identified using a GC-9710 equipped with a thermal conductivity detector (TCD) using a TDX-1 carbon molecular sieve packed column (2 m × 3 mm I.D.).

The heat values of the obtained oils were measured using an SHR-15B heat of combustion experimental device at room temperature, and the pressure of oxygen used was 2 MPa.

3. Results and discussion

3.1. Physicochemical properties

Fig. 1 shows the XRD patterns of the catalysts with different Ni/P ratios. The crystallite sizes of Ni_2P and $Ni_{12}P_5$ were calculated using the Scherrer equation, and the results are shown in Table 1. For Ni_xP/AC catalysts with Ni/P = 0.5 and 0.8, the XRD patterns exhibited only Ni_2P diffraction peaks at 2θ = 40.7°, 44.5°, 47.3°, 54.1°, 55.0°, 72.7°, and 74.7° (PDF 74-1385). As the Ni/P molar ratios increased to 1.0 and 1.5, diffraction peaks associated with $Ni_{12}P_5$ at 2θ = 38.3°, 41.7° and 48.9° (PDF 74-1381) were observed in addition to those of Ni_2P. As the Ni/P molar ratios increased from 1.0 to 1.5, the intensity of the $Ni_{12}P_5$ diffraction peaks strengthened. Interestingly, when the Ni/P molar ratio = 2.0, only $Ni_{12}P_5$ diffraction peaks were observed and the Ni_2P diffraction peaks (2θ = 44.5°, 47.1°, 54.1° and 56.2°) disappeared. Furthermore, new diffraction peaks assigned to crystalline metal Ni (PDF 70-1849) appeared at 44.4°, 51.7° and 76.3° along with those of $Ni_{12}P_5$ (2θ = 38.3°, 41.7°, 46.8° and 48.9°) when the Ni/P molar ratio was ≥3.0,

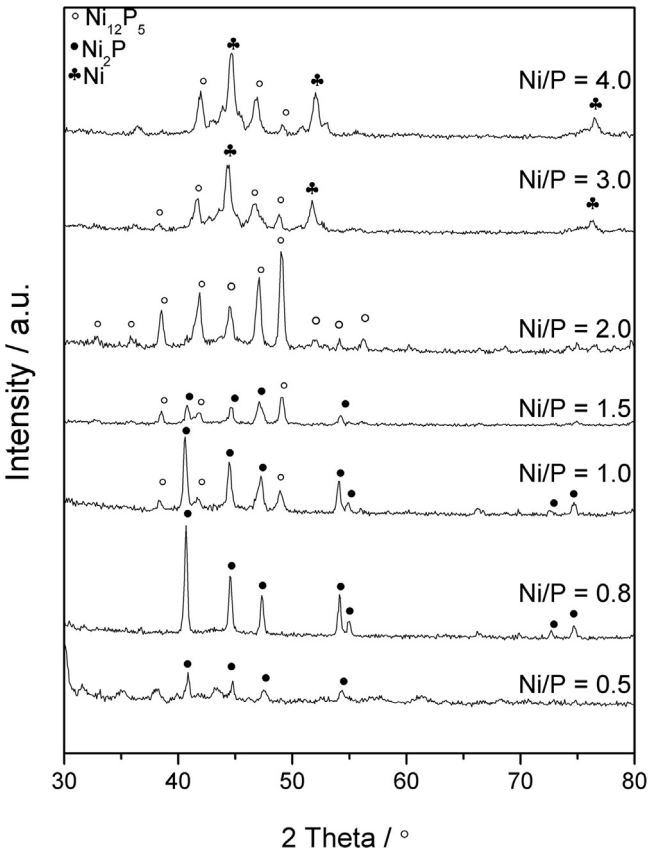

Fig. 1. XRD patterns for Ni_xP/AC catalysts with different Ni/P molar ratios. Ni crystals are designated by ♣, and $Ni_{12}P_5$ and Ni_2P are designated by ○ and ●, respectively. Intensity is given in arbitrary units (a.u.).

Table 1 shows the BET surface areas and the crystallite sizes of the Ni_xP_y phases based on the Scherrer's equation. For the Ni_xP/AC catalysts, the BET surface areas increased with increasing Ni/P molar ratio and reached the maximum at Ni/P = 2.0, but they gradually decreased when the Ni/P molar ratio was ≥3.0. N_2 sorption shown in Fig.S1(a) on series of Ni_xP/AC catalysts revealed type IV isotherms with a distinct hysteresis loop in the P/P_0 from 0.45 to 1.0, which is a typical characteristic of mesoporous material. The Barrett–Joyner–Halenda (BJH) pore-size distribution of all catalysts shown in Fig.S1(b) shows the pore diameter of catalysts between 10 and 40 nm, further indicating the mesoporous nature of the catalysts. In additon, the pore volumes of the catalysts increased with increasing Ni/P molar ratio and reached the maximum at Ni/P ≥ 2.0, indicating that Ni_2P first formed in the carrier channel. When Ni_2P and $Ni_{12}P_5$ coexisted on the surface of the support, the pore volume increased, which suggested that $Ni_{12}P_5$ could affect the distribution of Ni_2P. For the $Ni_{0.5}P$/AC and $Ni_{0.8}P$/AC catalysts, the Ni_2P crystallite size increased from 19.7 to 33.1 nm as the Ni/P molar ratio increased. With the formation of $Ni_{12}P_5$, the Ni_2P crystallite size gradually decreased from 22.1 to 18.2 nm at Ni/P molar ratios = 1.0 and 1.5. Furthermore, Ni_2P finally disappeared and only crystalline $Ni_{12}P_5$ was present at a Ni/P molar ratio = 2.0. However, the $Ni_{12}P_5$ crystallite size did not obviously change over the Ni/P molar ratio range of 1.0–2.0. Notably, the presence of Ni impeded the dispersion of $Ni_{12}P_5$, and the $Ni_{12}P_5$ crystallite size increased from 29.5 to 41.1 nm when the Ni/P molar ratio was ≥3.0. Therefore, the Ni_2P crystallite sizes were affected by the formation of

Table 1
Physicochemical data for the different Ni/P ratio catalysts.

Samples	The Ni/P ratio	BET surface area (m^2/g)	XRD Phase(s)	Pore volume (cm^3/g)	Crystal Size (nm)		Acid Amount
					Ni_2P	$Ni_{12}P_5$	S(461 K)/(542 K) a.u
$Ni_{0.5}P/AC$	0.5	356	Ni_2P	0.18	19.7	–	3708/3671
$Ni_{0.8}P/AC$	0.8	425	Ni_2P	0.21	33.1	–	2686/1758
$Ni_{1.0}P/AC$	1.0	544	Ni_2P,$Ni_{12}P_5$	0.26	22.1	22.4	2366/1562
$Ni_{1.5}P/AC$	1.5	574	Ni_2P,$Ni_{12}P_5$	0.35	18.2	22.9	995/0
$Ni_{2.0}P/AC$	2.0	601	$Ni_{12}P_5$	0.41	–	23.4	1083/0
$Ni_{3.0}P/AC$	3.0	584	Ni,$Ni_{12}P_5$	0.40	–	29.5	1406/0
$Ni_{4.0}P/AC$	4.0	499	Ni,$Ni_{12}P_5$	0.41	–	41.1	1560/0

–: The species was not detected.

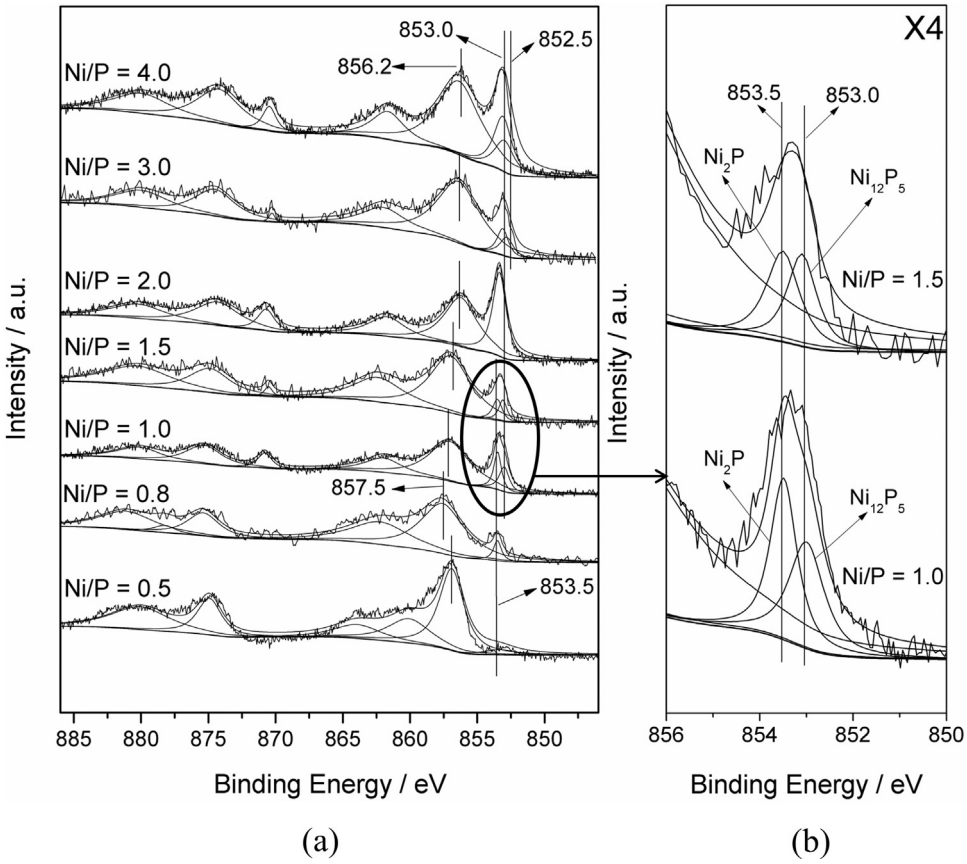

Fig. 2. (a) XPS spectra in the Ni (2p) regions for Ni_xP/AC catalysts with different Ni/P molar ratios. (b) Enlargement of part of $Ni_{1.0}P/AC$ and $Ni_{1.5}P/AC$ catalysts binding energy in 856–850 eV. (The number in the upmost right corner of the chart provides the peak amplification factor.)

$Ni_{12}P_5$, whereas the $Ni_{12}P_5$ crystalline sizes were affected by the presence of Ni. Based on the XRD and BET results, when the Ni/P molar ratio = 0.8 and 2.0, only pure Ni_2P crystallites and pure $Ni_{12}P_5$ crystallites were present on the support. Compared with our previous work, only pure Ni_2P crystallites formed on HZSM-22 with a Ni/P molar ratio = 1.0, but no pure $Ni_{12}P_5$ crystallite formed on HZSM-22 [8a]. According to the Boehm titration results, only carbonyl groups existed on the surface of the carbon, which might affect the formation of nickel phosphide species. This result indicated that the supports had an influence on the formation of nickel phosphide species.

The XPS spectra in the Ni (2p) and P (2p) regions for the Ni_xP/AC catalysts are shown in Figs. 2 (a) and 3, respectively. All spectra were decomposed by considering the spin-orbit splitting of the Ni ($2p_{3/2}$) and Ni ($2p_{1/2}$) lines (17 eV) and the shake-up peaks at approximately 5 eV higher than the binding energy of the parent signal. The spectrum for $Ni_{0.5}P/AC$ was similar to that for the $Ni_{0.8}P/AC$ catalyst, and the peaks at approximately 857.5 eV and 135.0 eV were assigned to Ni^{2+} and P^{5+} species in PO_4^{3-}, respectively [24]. The peaks observed at 853.5 and approximately 130.2 eV were attributed to reduced Ni and P species, respectively. These binding energies indicated that the Ni in Ni_2P had a partial positive charge (δ^+), where $0 < \delta < 2$, whereas the reduced P had a smaller electron binding energy than elemental P (130.4) [25], indicating that the P had a partial negative charge (δ^-), where $0 < \delta < 1$ [24]. The XPS spectrum for the $Ni_{1.0}P/AC$ catalyst was similar to that for the $Ni_{1.5}P/AC$ catalyst, and the Ni ($2p_{3/2}$) peaks at 853.5 and 853.0 eV were assigned to $Ni^{\delta+}$ in Ni_2P and $Ni_{12}P_5$, respectively. The quantitative results showed that the surface content of Ni_2P was larger than that of $Ni_{12}P_5$ on $Ni_{1.0}P/AC$ (approximately 1.3/1), whereas the Ni_2P surface content was equal to that of $Ni_{12}P_5$ on $Ni_{1.5}P/AC$ (approximately 1/1) as shown in Fig. 2(b) [24,26]. For the $Ni_{2.0}P/AC$ catalyst, the peak at 853.0 eV was attributed to $Ni^{\delta+}$ in $Ni_{12}P_5$. For the $Ni_{3.0}P/AC$ and $Ni_{4.0}P/AC$ catalysts, the Ni ($2p_{3/2}$) peaks at 852.5 eV had a lower binding energy than that of reduced Ni in Ni_2P and $Ni_{12}P_5$, which was attributed to the Ni°, and the Ni

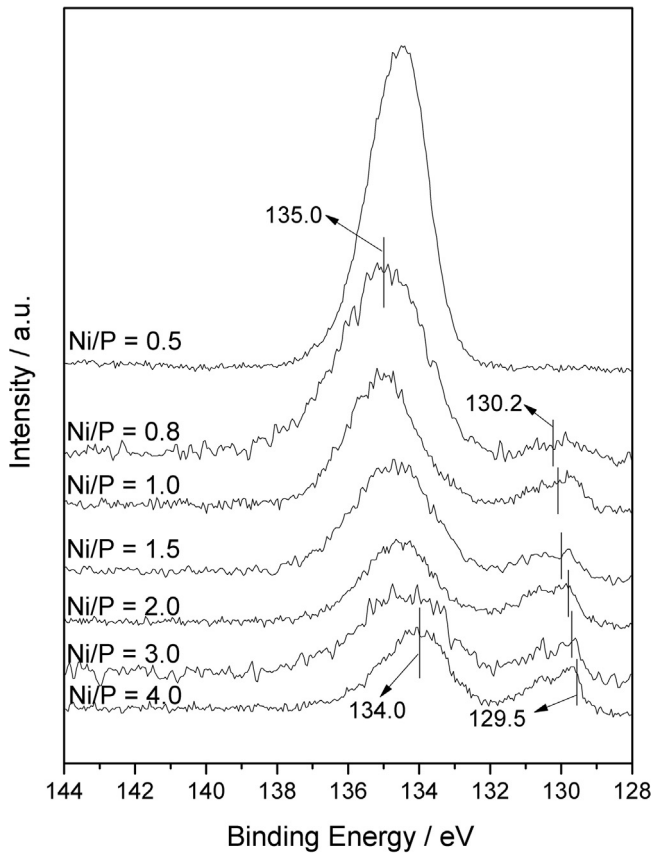

Fig. 3. XPS spectra in the P (2p) regions for Ni_xP/AC catalysts with different Ni/P molar ratios.

($2p_{3/2}$) peaks at 853.0 eV was assigned to $Ni^{\delta+}$ in $Ni_{12}P_5$, whereas the P ($2p_{3/2}$) peak at 129.5 eV was assigned to $P^{\delta-}$ in $Ni_{12}P_5$. The magnitude of δ was quite small, as the Ni ($2p_{3/2}$) binding energies of 853.5 and 853.0 eV were closed to that of Ni metal (852.5–852.9) [27]. Therefore, the magnitude of δ in Ni_2P was larger than in $N_{12}P_5$. For all of the catalysts, the Ni ($2p_{3/2}$) binding energies characteristic for Ni^{2+} decreased from 857.5 to 856.2 eV and the P ($2p_{3/2}$) binding energies characteristic for P^{5+} decreased from 135.0 to 134.0 eV, suggesting the formation of low valence Ni and P. Furthermore, the Ni ($2p_{3/2}$) binding energies characteristic for nickel atoms in Ni_xP_y decreased from 853.5 to 853.0 eV, relating to Ni_2P and $Ni_{12}P_5$ (Fig. 2(a)), respectively. Accordingly, the binding energies characteristic for P atoms in Ni_xP_y phases shifted in the opposite direction from 130.2 to 129.5 eV (as the amount of P decreased). The above results were in good agreement with the shift of binding energies detected in reference [24,28] for Ni_2P and $Ni_{12}P_5$. They were evidence for less transfer of electron density from Ni to P atoms as the Ni/P molar ratio increased from 0.8 to 4.0 in the Ni_xP/AC catalysts. This result corresponded to the enhancement of metallicity of nickel atoms in the sequence $Ni_{12}P_5 > Ni_2P$, yielding a corresponding increase of their reactivity relative to oxygen, therefore $Ni_{12}P_5$ was more favor for oxygen removal [28].

Fig. 4A–C shows the morphology images of the AC support, $Ni_{0.5}P$/AC, and $Ni_{0.8}P$/AC. A large number of Ni_2P were observed to be supported on AC; furthermore, the Ni_2P crystallites exhibited poor dispersion. In contrast, as the Ni/P molar ratio increased to 1.0 and 1.5, the Ni_2P and $Ni_{12}P_5$ exhibited a spherical shape with good dispersion as shown in Fig. 4D and E, presumably due to the presence of $Ni_{12}P_5$. The TEM images of $Ni_{0.5}P$/AC and $Ni_{0.8}P$/AC show aggregation of Ni_2P in Fig. 4B and C, while Ni_2P coexisted with $Ni_{12}P_5$ in the $Ni_{1.0}P$/AC and $Ni_{1.5}P$/AC catalysts dispersed well on the carbon surface, as shown in Fig. 4D and E. The highest dispersion of Ni_xP_y was observed on the $Ni_{1.5}P$/AC catalyst. The high-resolution image of $Ni_{1.5}P$/AC revealed that Ni_2P adopted a globular morphology on the carbon support. The Ni_2P particle had a diameter of 18 nm and the *d*-spacing was approximately 1.70 Å, as shown in Fig. 5, which was consistent with the {300} crystallographic plane of Ni_2P, as determined by comparison with the JCPDS power diffraction file (card no.74-1385). EDX-mapping analysis (shown in Fig. 5) of $Ni_{1.5}P$/AC further confirmed the presence and good dispersion of Ni and P elements. Note that Ni_2P disappeared on $Ni_{2.0}P$/AC catalyst and $Ni_{12}P_5$ aggregated to some extent, as shown in Fig. 4F. Therefore, the degree of $Ni_{12}P_5$ dispersion on the $Ni_{2.0}P$/AC catalyst was poorer than that on the $Ni_{1.0}P$/AC and $Ni_{1.5}P$/AC catalysts where Ni_2P and $Ni_{12}P_5$ coexisted. When the Ni/P molar ratio increased to 3.0 and 4.0, a new Ni phase formed and $Ni_{12}P_5$ aggregated into larger particles, as shown in Fig. 4G and H. For all catalysts, the highest dispersion was observed on the $Ni_{1.5}P$/AC catalyst, where the surface content of $Ni_{12}P_5$ was approximately equal to that of Ni_2P based on the XPS results. The TEM images revealed a more homogeneous particle distribution on the $Ni_{1.0}P$/AC and $Ni_{1.5}PA/C$ catalysts than that on the other catalysts. The particle size ranged from approximately 12.2 to 43.6 nm, as observed by TEM, which was consistent with the particle size range of 18.2–41.1 nm determined by XRD. Based on the above TEM and XPS results, it was concluded that the interaction between Ni_2P and $Ni_{12}P_5$ could induce better dispersion of Ni_2P and $Ni_{12}P_5$ and that $Ni_{12}P_5$ had a favorable effect on the formation of highly dispersed Ni_2P.

Fig. 6 shows the NH_3-TPD profiles of all of the Ni_xP/AC catalysts, and the amounts of surface acids are listed in Table 1. The NH_3-TPD profiles of $Ni_{0.5}P$/AC, $Ni_{0.8}P$/AC and $Ni_{1.0}P$/AC consisted of one strong peak at approximately 460 K (low temperature) and a less intense peak at approximately 542 K (high temperature), which corresponded to the weak Brønsted acid sites and strong Lewis acid sites, respectively [29]. However, the NH_3-TPD profiles of $Ni_{1.5}P$/AC, $Ni_{2.0}P$/AC, $Ni_{3.0}P$/AC, and $Ni_{4.0}P$/AC consisted of only one peak at approximately 460 K (low temperature), indicating that the $Ni_{1.5}P$/AC, $Ni_{2.0}P$/AC, $Ni_{3.0}P$/AC, and $Ni_{4.0}P$/AC catalysts had only weak Brønsted acid sites and that the Lewis acid sites disappeared. The Brønsted acid sites were attributed to the surface P—OH groups [18a], and the high-temperature shoulder at approximately 542 K for the $Ni_{0.5}P$/AC, $Ni_{0.8}P$/AC and $Ni_{1.0}P$/AC catalysts corresponded to NH_3 absorption by $Ni^{\delta+}$ ($0 < \delta < 1$) ions in the nickel phosphide phase. The strong adsorption of NH_3 molecules by the nickel phosphide phase was caused by their complexation with surface nickel atoms involving their d-orbitals and lone electron pairs of nitrogen atoms. Furthermore, the magnitude of δ in Ni_2P was larger than in $N_{12}P_5$ [24]. The Ni_2P phase should be more favorable for the complexation formation of $[Ni(NH_3)_4]^{2+}$ than the $Ni_{12}P_5$ phase.

3.2. Catalytic activity

Before catalytic activity experiment, $Ni_{1.5}P$/AC catalyst was selected to perform kinetic test, and the results were shown in Fig. S(2–4). Based on the results of kinetic test, the reaction time was selected 2.5 h, in addition to this, 3 g catalysts and the particle size of 40–60 mesh could eliminate the influence of external diffusion and internal diffusion, respectively. The deoxygenation reactions of palmitic acid over the Ni_xP/AC catalysts were performed in a special fixed-bed reactor [8a], and the results are shown in Table 2. For the $Ni_{0.5}P$/AC and $Ni_{0.8}P$/AC catalysts, the products were solid accompanied by the palmitic acid, and the conversion of palmitic acid was 86.2 and 86.3%, respectively. The gaseous products were primarily composed of CO, CO_2, CH_4, and C_2H_6, as determined by GC analysis. It was considered that Lewis acid sites were beneficial to the hydrocracking reaction. These results were in good agreement with those of a previous study [8a]. The conversion of palmitic acid

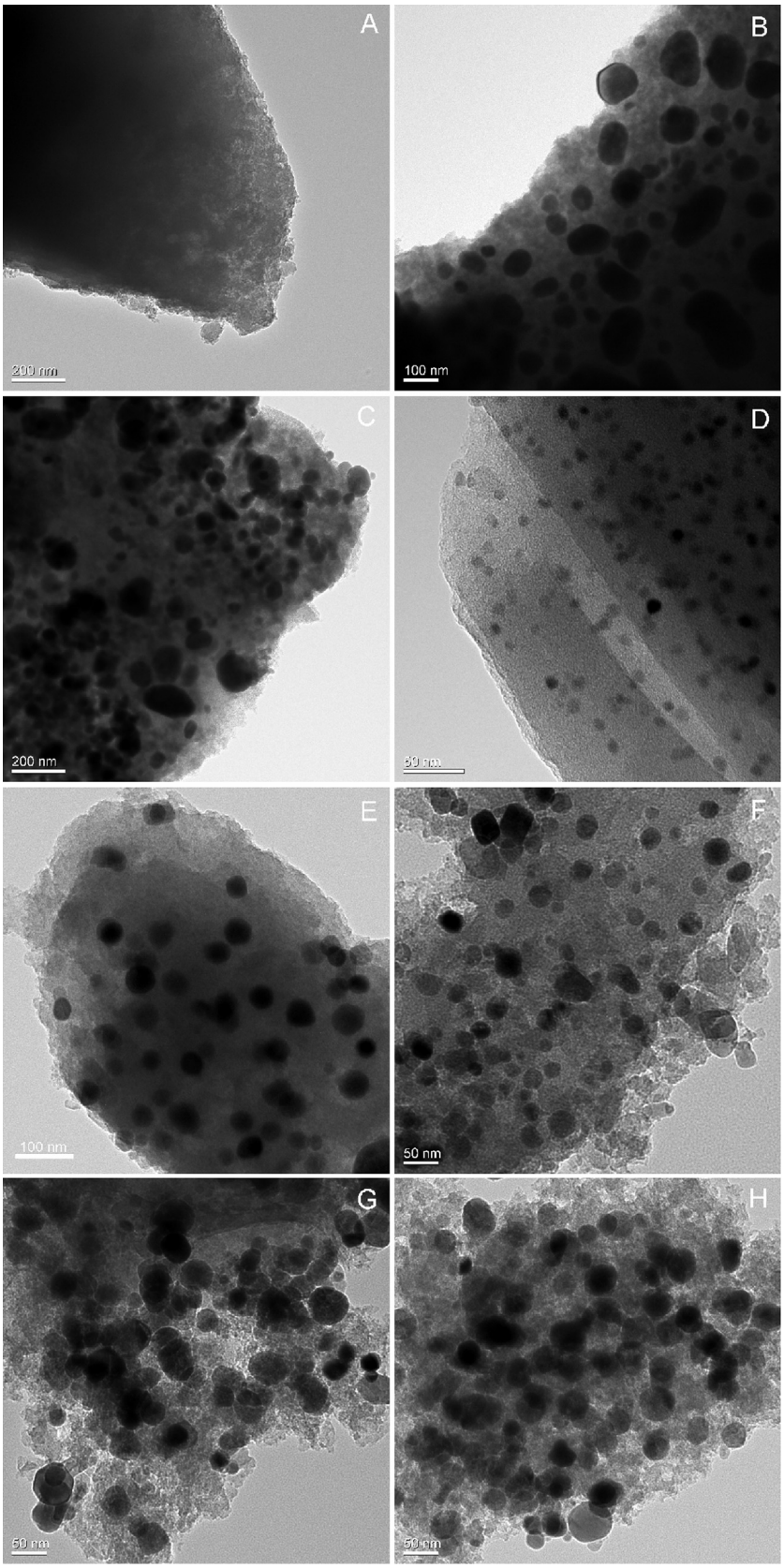

Fig. 4. TEM images of (A) AC, (B) $Ni_{0.5}P/AC$, (C) $Ni_{0.8}P/AC$, (D) $Ni_{1.0}P/AC$, (E) $Ni_{1.5}P/AC$, (F) $Ni_{2.0}P/AC$, (G) $Ni_{3.0}P/AC$, (H) $Ni_{4.0}P/AC$.

reached 100% with a Ni/P molar ratio of ≥1.0. Furthermore, the maximum oil yield reached 56.0% over the $Ni_{1.5}P/AC$ catalyst and the heat value of the product oil was 46.5 MJ kg^{-1}. If the palmitic acid were completely converted to pentadecane by decarboxylation and decarbonylation, the maximum theoretical pentadecane yield would be 82.8%. In the results shown in Table 2, all of the oil yields were lower than the maximum theoretical oil yield, primarily because of the hydrocracking reaction. When the Ni/P molar ratio

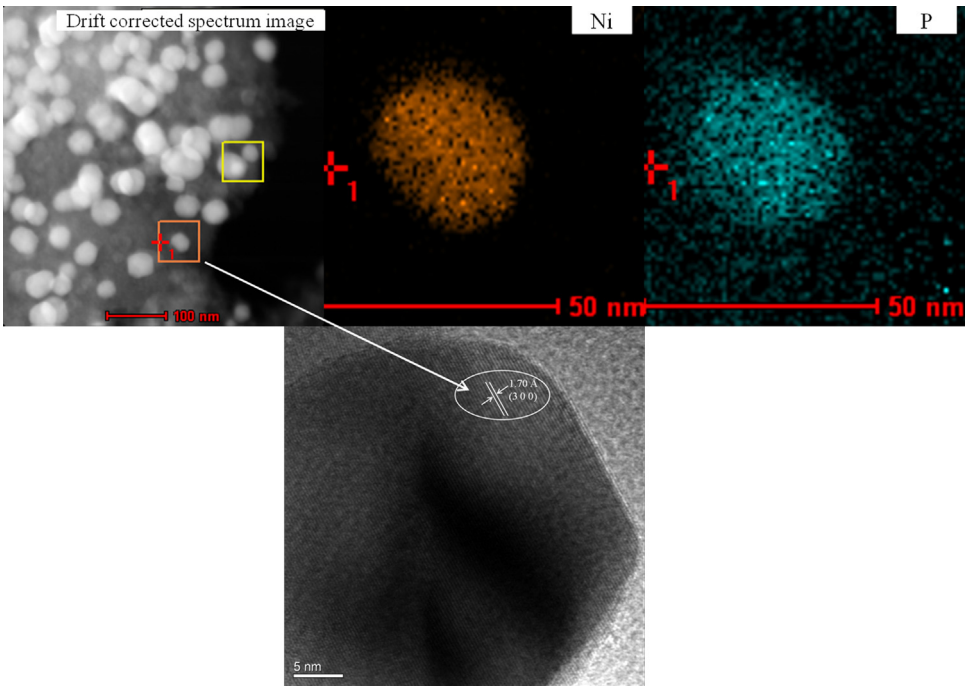

Fig. 5. Edx-mapping and high-resolution TEM micrographs of $Ni_{1.5}P$/AC.

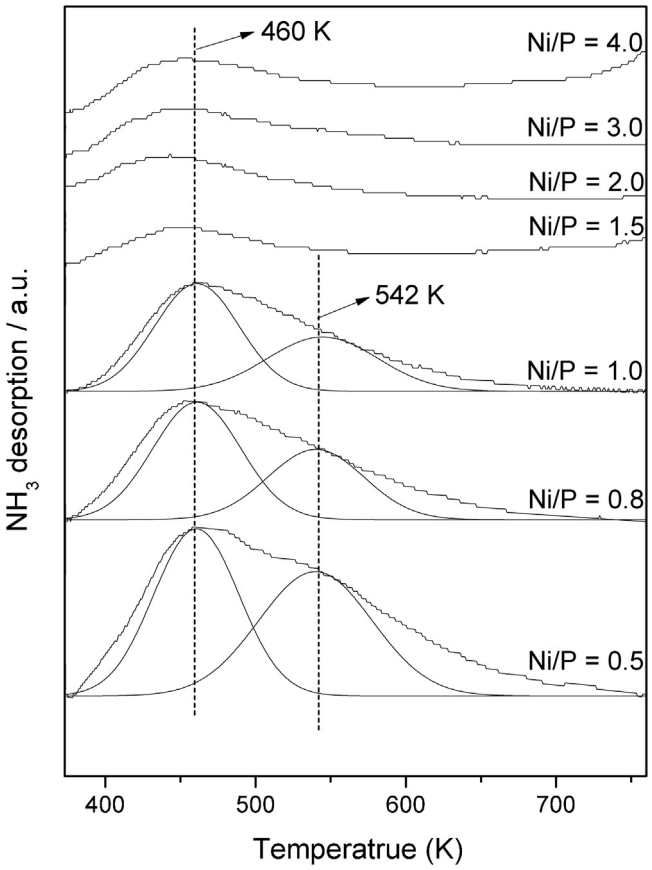

Fig. 6. NH_3-TPD profiles of Ni_xP/AC catalysts with different Ni/P molar ratios.

increased to 3.0, the oil yield clearly decreased, which might be due to the increase in the $Ni_{12}P_5$ crystalline size (29.5 nm) and to the formation of crystalline Ni. It is known that crystalline Ni favors for the cracking reaction [16]. In addition, we found that the $Ni_{12}P_5$ crystallite size of 20–24 nm was beneficial to the decarboxylation and decarbonylation of palmitic acid and the enhancement of oil yield in our previous study [8a]. Furthermore, Fig. 7 also indicates that the crystallite size of $Ni_{12}P_5$ was correlated to the oil yield, and the highest oil yield was 56.0% when the crystallite size of $Ni_{12}P_5$ was approximately 22.9 nm. As the crystallite size of $Ni_{12}P_5$ increased, the oil yield decreased. In addition, the oil yield depended on the density and strength of acid sites of the catalysts. Typically the yield of oil decreased with increasing concentrations and strengths of acid sites, because over-cracking yielded gaseous products [18b]. Combined with NH_3-TPD results in Table 1 and activity results in Table 2, it could be found that when the acid amount decreased, the oil yield increased. However, the oil yield on $Ni_{4.0}P$/AC catalyst was slightly lower than on $Ni_{1.0}P$/AC, which might be attributed to the Ni species existed on $Ni_{4.0}P$/AC catalyst. Chen et al. have confirmed that Ni catalyst showed much higher cracking activity compared to the nickel phosphide catalysts [18a].

Table 2
The activity test results of the conversion of palmitic acid on different Ni/P molar ratios catalysts and the obtained diesel heat value.

Ni/P	0.5:1	0.8:1	1.0:1	1.5:1	2.0:1	3:1	4:1
Conversion (%)	86.2	86.3	99.4	100.0	100.0	100.0	100.0
Oil yield (%)	–	–	43.4	56.0	53.2	43.6	41.4
C_{15} Selective (%)	54.6	57.0	74.9	56.7	53.8	52.3	40.1
HV (MJ kg^{-1})	46.0	46.1	46.4	46.5	46.2	45.2	45.0

–: The products are solid, and there is not oil.

Figs. 8 and 9 show the GC–MS chromatographs and the distribution of products, and the composition of products from the conversion of palmitic acid over all catalysts shown in Table S1. For the $Ni_{0.5}P$/AC and $Ni_{0.8}P$/AC catalysts, the solid products are composed of the unconverted palmitic acid, and some $C_{11}H_{24}$-$C_{15}H_{32}$ linear chain alkanes and alkenes absorbed by palmitic acid. In the mixture products, there were ca. 4% C_{11}-C_{14} linear chains, ca. 55% and 57% C_{15} linear chains, and ca. 16% and 15% alkenes according to GC–MS analysis over $Ni_{0.5}P$/AC and $Ni_{0.8}P$/AC catalysts, respectively. When the Ni/P molar ratio increased to 1.0 and 1.5, $C_{11}H_{24}$-$C_{15}H_{32}$ linear chain alkanes

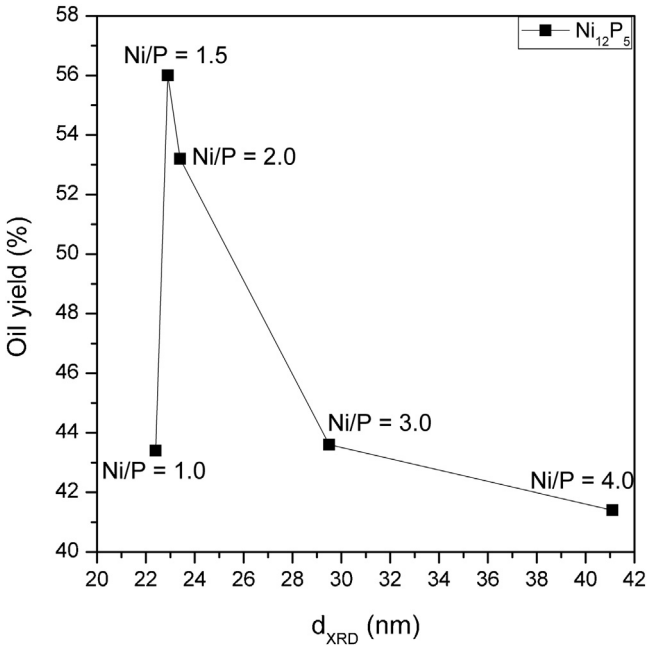

Fig. 7. The crystallite sizes of $Ni_{12}P_5$ corresponding to the oil yield.

and alkenes were observed, and unconverted palmitic acid disappeared. Notably, branched alkanes were present, as shown in Fig. 8. The product distributions over the $Ni_{1.0}P$/AC and $Ni_{1.5}P$/AC catalysts were different, as shown in Fig. 9. For the $Ni_{1.0}P$/AC catalyst, the product contained ca.11% C_{11}-C_{14} linear chains, 75% C_{15} linear chains, 5% alkenes, 5% branched alkanes, and 4% other hydrocarbons. For the $Ni_{1.5}P$/AC catalyst, the product contained ca.7% C_{11}-C_{14} linear chains, 57% C_{15} linear chains, 21% alkenes, 3% branched alkanes, 8% cyclanes (cyclenes), 4%

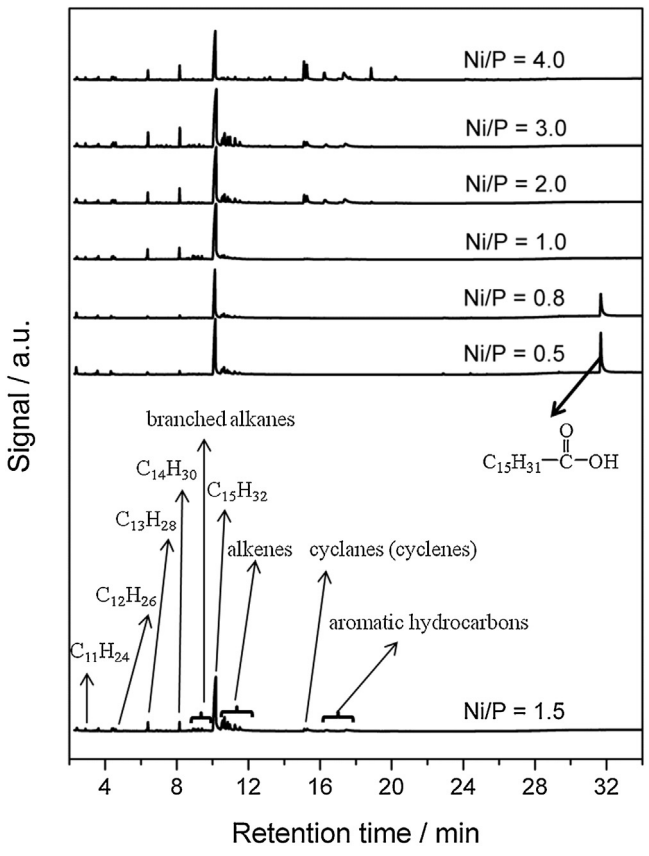

Fig. 8. GC–MS chromatographs of products at 623 K, 5% H_2/Ar with a flow rate of 30 mL/min.

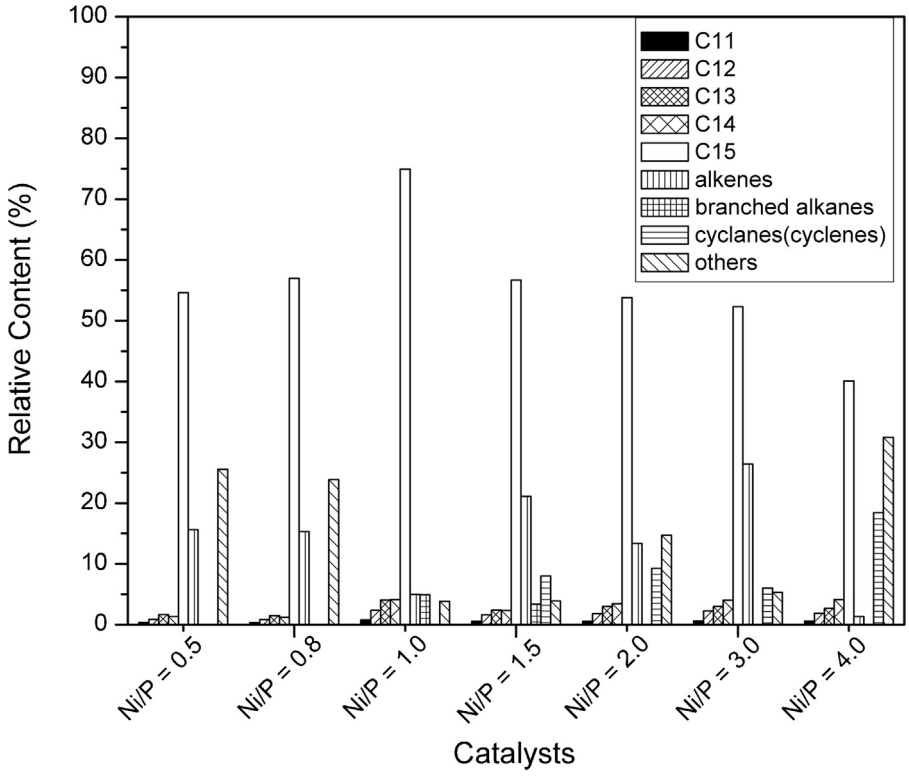

Fig. 9. Product distributions of hydrocarbons over a series of Ni_xP/AC catalysts at 623 K, 5% H_2/Ar with a flow rate of 30 mL min^{-1}.

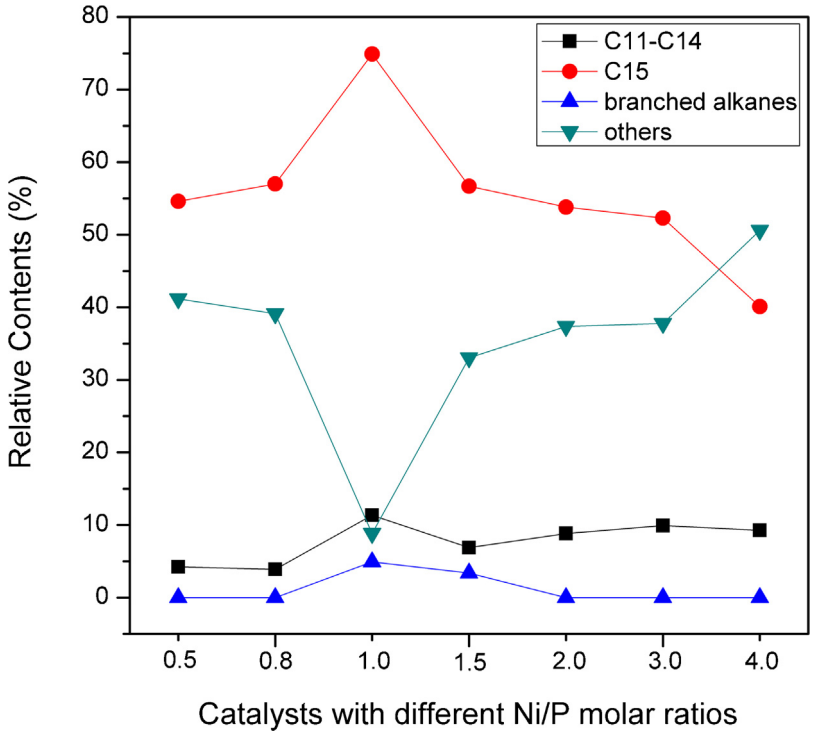

Fig. 10. The main product distributions of hydrocarbons over the catalysts with different Ni/P molar ratios at 623 K, 5% H_2/Ar with a flow rate of 30 mL min^{-1}. Others mainly included palmitic acid, alkenes, cyclanes (cyclenes) and aromatic alkanes.

other hydrocarbons (including 2% aromatic hydrocarbons). In addition, the C_{15} selectivity on the $Ni_{1.0}P$/AC catalyst was the highest among the catalysts. When the Ni/P molar ratio increased to 2.0, 3.0 and 4.0, the branched alkanes disappeared again and the other products were still present (shown in Fig. 8). The product over the $Ni_{2.0}P$/AC catalyst included 9% C_{11}-C_{14} linear chains, 54% C_{15} linear chains, 13% alkenes, 9% cyclanes (cyclenes) and 15% other hydrocarbons (including 12% aromatic hydrocarbons). For the $Ni_{3.0}P$/AC and $Ni_{4.0}P$/AC catalysts, the product categories were the same as the products over the $Ni_{2.0}P$/AC catalyst, but the amount of every substance was different (shown in Table S1). It was noted that branched alkanes, cyclanes (cyclenes) and aromatic hydrocarbons coexisted with a Ni/P molar ratio = 1.5, thus the high-grade diesel was obtained on the $Ni_{1.5}P$/AC catalyst. For the phase-pure Ni_2P containing the $Ni_{0.8}P$/AC and $Ni_{0.5}P$/AC catalysts, the selectivity of $C_{15}H_{32}$ was higher compared to the phase-pure $Ni_{12}P_5$ containing the $Ni_{2.0}P$/AC catalyst. The highest $C_{15}H_{32}$ selectivity of 74.9% was obtained over the $Ni_{1.0}P$/AC catalyst as shown in Table 2. The coexistence of Ni_2P and $Ni_{12}P_5$ on the $Ni_{1.0}P$/AC catalyst might be responsible for the highest selectivity of $C_{15}H_{32}$. Furthermore, the oil yield on phase-pure $Ni_{12}P_5$ of the $Ni_{2.0}P$/AC catalyst slightly decreased compared with $Ni_{1.5}P$/AC, and the oil yield was the highest (56.0%) over $Ni_{1.5}P$/AC. However, the oil yield obtained was only 44.2% over (1:1 mass ratio) mechanical mixture of $Ni_{0.8}P$/AC + $Ni_{2.0}P$/AC. Therefore, we reasonably speculated that there was a synergetic effect of $Ni_{12}P_5$ and Ni_2P on the deoxygenation of palmitic acid. To further attest the synergetic effect of $Ni_{12}P_5$ and Ni_2P, the CO chemisorption and CO-TPD experiments were performed. CO chemisorption and CO-TPD experiments over $Ni_{0.8}P$/AC, $Ni_{2.0}P$/AC, (1:1 mass ratio) mechanical mixture of $Ni_{0.8}P$/AC + $Ni_{2.0}P$/AC, and $Ni_{1.5}P$/AC catalysts were performed by using CO as probe molecule. The CO-TPD profiles of all catalysts are shown in Fig. S5. It was observed that the CO-TPD profiles of $Ni_{0.8}P$/AC, $Ni_{2.0}P$/AC and mechanical mixture catalysts of $Ni_{0.8}P$/AC + $Ni_{2.0}P$/AC had CO desorption peak at approximately 370 K. However, the CO-TPD profiles of $Ni_{1.5}P$/AC had an intense CO desorption peak at 333 K, which was obviously different from those of $Ni_{0.8}P$/AC, $Ni_{2.0}P$/AC, $Ni_{0.8}P$/AC + $Ni_{2.0}P$/AC mechanical mixture catalysts. The CO desorption temperature over $Ni_{1.5}P$/AC was the lowest compared with the others catalysts, which indicated that the synergetic effect between crystalline Ni_2P and $Ni_{12}P_5$. Table S2 shows the CO chemisorption capacity of $Ni_{0.8}P$/AC, $Ni_{2.0}P$/AC, $Ni_{0.8}P$/AC + $Ni_{2.0}P$/AC (mechanical mixture), and $Ni_{1.5}P$/AC catalysts. The amount of adsorbed CO was the higher over $Ni_{1.5}P$/AC catalyst relative to the other three types of catalysts, and the amount of adsorbed CO on $Ni_{0.8}P$/AC, $Ni_{2.0}P$/AC and $Ni_{0.8}P$/AC + $Ni_{2.0}P$/AC (mechanical mixture) were approximately the same, as shown in Table S2. Based on the above results, we reasonably speculated that the crystalline Ni_2P and $Ni_{12}P_5$ had a synergetic effect on the surface of activated carbon, and the synergetic effect accounted for the high catalytic activity of $Ni_{1.5}P$/AC catalysts. Furthermore, $Ni_{12}P_5$ and Ni_2P coexisting on the surface of carbon supports could be favorable for the branched alkanes formation, which might improve the octane rating. When the Ni/P molar ratio exceeded 1.5, the branched alkanes disappeared, and aromatic hydrocarbons were generated over the $Ni_{1.5}P$/AC, $Ni_{2.0}P$/AC, $Ni_{3.0}P$/AC, and $Ni_{4.0}P$/AC catalysts, which could be correlated to the Brønsted acid sites alone. Based on a previous study [8a], we attested that Brønsted acid sites alone were responsible for the isomerization reactions. The synergetic effect of $Ni_{12}P_5$ and Ni_2P played a crucial role in the deoxygenation process.

Fig. 10 shows the relationship between the distribution of the main products and the Ni/P molar ratios. It could be observed that the C_{11}-C_{14} linear chain alkanes, C_{15} linear chain alkanes, and branched alkanes contents were the highest with a Ni/P molar ratio = 1.0, whereas the contents of the other products (except for branched alkanes, C_{11}-C_{14} and C_{15} linear chain alkanes) were the lowest. The above results suggested that the synergetic effect of $Ni_{12}P_5$ and Ni_2P on the deoxygenation process of palmitic

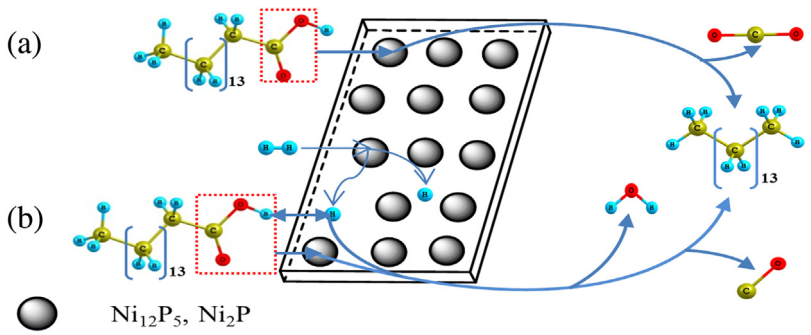

Scheme 2. The main catalytic pathways proposed for the deoxygenation of palmitic acid on $Ni_{1.5}P$/AC. Ni_xP_y represents $Ni_{12}P_5$ or Ni_2P. The pathways are (a) decarboxylation and (b) decarbonylation.

acid was favorable for the C_{15} selectivity and branched alkanes formation.

3.3. The main catalytic pathways of palmitic acid over $Ni_{1.5}$/AC catalyst

In our previous study, we found that the catalytic pathways of palmitic acid on Ni_xP/H-ZSM-22 were very complicated, which led to the fact that the product components were also very complex and the C_{15} selectivity was low [8a]. However, our present study suggested that the C_{15} selectivity could be clearly improved by controlling the formation of nickel phosphide species on a carbon support. Considering the above activity results and the absence of C_{16} in the products, we reasonably speculated that the $Ni_{12}P_5/Ni_2P$ active sites of Ni_xP/AC preferentially catalyzed the decarboxylation and decarbonylation reactions during the conversion of palmitic acid. Based on the above experimental results, the deoxygenation of palmitic acid over $Ni_{1.5}$/AC primarily proceeds through two pathways, as shown in Scheme 2. One is the direct decarboxylation pathway, i.e., carboxyl of palmitic acid is activated over the $Ni_{12}P_5/Ni_2P$ active phase on the carbon surface, and then palmitic acid is directly converted into pentadecane and CO_2 by decarboxylation (Scheme 2a), whereas the other is the decarbonylation pathway, i.e., H_2 is first dissociated over $Ni_{12}P_5/Ni_2P$ active sites, and the dissociated H combines with the OH of palmitic acid to form H_2O, generating $C_{14}H_{29}$-CH_2-CHO as an intermediate. Finally, the intermediate is further converted to pentadecane by decarbonylation (Scheme 2b).

The above plausible deoxygenation pathways might simultaneously occur and alter each other over $Ni_{1.5}P$/AC. The intermediates from decarbonylation and decarboxylation, such as pentadecane and $C_{14}H_{29}$-CH_2-CHO, might undergo isomerization and hydrocracking reactions due to the acid sites. The obtained high-grade diesel resulted from the aggregation of the above processes.

4. Conclusions

For Ni_xP/AC catalysts with Ni/P = 0.5 and 0.8, only pure Ni_2P crystallites formed on the AC. As the Ni/P ratio increased to 1.0 and 1.5, the significant $Ni_{12}P_5$ were present in addition to Ni_2P and that $Ni_{12}P_5$ profitably affected the Ni_2P dispersion on the AC. Whereas the Ni_2P crystallites disappeared and only pure $Ni_{12}P_5$ crystallites formed when Ni/P = 2.0. Furthermore, as the Ni/P molar ratio increased to 3.0 and 4.0, the new crystalline Ni formed in addition to $Ni_{12}P_5$. The conversion of palmitic acid was 100% on the $Ni_{1.5}P$/AC catalyst in a fixed-bed reactor under ambient pressure in the absence of any solvents, and a high oil yield of 56.0% with a high heating value of 46.5 MJ kg^{-1} were obtained. The main products were C_{15} linear chains, in addition to some C_{11}-C_{14} linear chains, alkenes, branched alkanes, cyclanes (cyclenes) and aromatic hydrocarbons. Because of the synergetic effect of $Ni_{12}P_5$ and Ni_2P on the deoxygenation of palmitic acid and their high dispersion, the saturated fatty acid could be converted into diesel with a high conversion, high oil yield, and high heating value.

Acknowledgements

This work was financially supported by the National Natural Science Foundation of China (No. 21303109) and by the Application Foundation Program of Sichuan Province (No. 2013JY0007).

Appendix A. Supplementary data

Supplementary data associated with this article can be found, in the online version, at http://dx.doi.org/10.1016/j.apcatb.2016.01.051.

References

[1] G. Huber, A. Corma, Angew. Chem. Int. Ed. 46 (2007) 7184–7201.
[2] E. Kunkes, D. Simonetti, R. West, J. Serrano-Ruiz, C. Gärtner, J. Dumesic, Science 322 (2008) 417–421.
[3] S. Lestari, P. Mäki-Arvela, J. Beltramini, G. Lu, D. Murzin, ChemSusChem 2 (2009) 1109–1119.
[4] (a) C. Zhao, J. Lercher, Angew Chem. Int. Ed. 51 (2012) 5935–5940; (b) M. Peroni, G. Mancino, E. Baráth, O. Gutiérrez, J. Lercher, Appl. Catal. B: Environ. 180 (2016) 301–311.
[5] (a) C. Wang, Z. Tian, L. Wang, R. Xu, Q. Liu, W. Qu, H. Ma, B. Wang, ChemSusChem 5 (2012) 1974–1983; (b) R. Kukushkin, O. Bulavchenko, V. Kaichev, V. Yakovlev, Appl. Catal. B: Environ. 163 (2015) 531–538.
[6] (a) N. Chen, S. Gong, E. Qian, Appl. Catal. B: Environ. 174–175 (2015) 253–263; (b) J. Immer, M. Kelly, H. Lamb, Appl. Catal. A: Gen. 375 (2010) 134–139.
[7] (a) B. Peng, C. Zhao, S. Kasakov, S. Foraita, J. Lercher, Chem. Eur. J. 19 (2013) 4732–4741; (b) C. Kordulis, K. Bourikas, M. Gousi, E. Kordouli, A. Lycourghiotis, Appl. Catal. B: Environ. 181 (2016) 156–196.
[8] (a) Y. Liu, L. Yao, H. Xin, G. Wang, D. Li, C. Hu, Appl. Catal. B: Environ. 174–175 (2015) 504–514; (b) R.H. Bowker, B. Ilic, B.A. Carrillo, M.A. Reynolds, B.D. Murray, M.E. Bussell, Appl. Catal. A: Gen. 482 (2014) 221–230.
[9] J. Fu, F. Shi, L. Thompson, X. Lu, P. Savage, ACS Catal. 1 (2011) 227–231.
[10] B. Smith, H. Greenwell, A. Whiting, Energy Environ. Sci. 2 (2009) 262–271.
[11] I. Simakova, O. Simakova, A. Romanenko, D. Murzin, Ind. Eng. Chem. Res. 47 (2008) 7219–7225.
[12] J. Lopez-Ruiz, R. Davis, Green Chem. 16 (2014) 683–694.
[13] J. Fu, X. Lu, P. Savage, Energy Environ. Sci. 3 (2010) 311–317.
[14] J. Fu, X. Lu, P. Savage, ChemSusChem 4 (2011) 481–486.
[15] M. Snåre, I. Kubičková, P. Mäki-Arvela, K. Eränen, D. Murzin, Ind. Eng. Chem. Res. 45 (2006) 5708–5715.
[16] E. Santillan-Jimenez, T. Morgan, J. Lacny, S. Mohapatra, M. Crocker, Fuel 103 (2013) 1010–1017.
[17] Y. Yang, C. Ochoa-Hernández, V. de la Peña O'shea, J. Coronado, D. Serrano, ACS Catal. 2 (2012) 592–598.
[18] (a) J. Chen, H. Shi, L. Li, K. Li, Appl. Catal. B: Environ. 144 (2014) 870–884; (b) S. Katikaneni, J. Adjaye, N. Bakhshi, Energy Fuels 9 (1995) 599–609.
[19] K. Li, R. Wang, J. Chen, Energy Fuels 25 (2011) 854–863.
[20] J. Cecilia, A. Infantes-Molina, E. Rodríguez-Castellón, A. Jiménez-López, S. Oyama, Appl. Catal. B: Environ. 136–137 (2013) 140–149.
[21] H. Shi, J. Chen, Y. Yang, S. Tian, Fuel Process. Technol. 118 (2014) 161–170.

[22] Y. Zeng, B. Zhao, L. Zhu, D. Tong, C. Hu, RSC Adv. 3 (2013) 10806–10816.
[23] T. Korányi, A. Coumans, E. Hensen, R. Ryoo, H. Kim, É. Pfeifer, Z. Kasztovszky, Appl. Catal. A: Gen. 365 (2009) 48–54.
[24] S. Sawhill, K. Layman, D. Van Wyk, M. Engelhard, C. Wang, M. Bussell, J. Catal. 231 (2005) 300–313.
[25] R. Franke, T. Chassé, P. Streubel, A. Meisel, J. Electron Spectrosc. Relat. Phenom. 56 (1991) 381–388.
[26] S. Sawhill, D. Phillips, M. Bussell, J. Catal. 215 (2003) 208–219.
[27] C. Wagner, D. Briggs, M. Seah (Eds.), Practical Surface Analysis by Auger and X-ray Photoelectron Spectroscopy, John Wiley & Sons, New York, 1983, p. 495.
[28] M. Landau, M. Herskowitz, T. Hoffman, D. Fuks, E. Liverts, D. Vingurt, N. Froumin, Ind. Eng. Chem. Res. 48 (2009) 5239–5249.
[29] R. Zarchin, M. Rabaev, R. Vidruk-Nehemya, M. Landau, M. Herskowitz, Fuel 139 (2015) 684–691.